Nano Energy 54 (2018) 390–399

Contents lists available at ScienceDirect

Nano Energy

journal homepage: www.elsevier.com/locate/nanoen

Full paper

Photothermally tunable biodegradation of implantable triboelectric nanogenerators for tissue repairing

Zhe Li[a,b,1], Hongqing Feng[a,b,1], Qiang Zheng[a,b], Hu Li[a], Chaochao Zhao[a,b], Han Ouyang[a,b], Sehrish Noreen[a], Min Yu[a], Fan Su[e], Ruping Liu[e], Linlin Li[a,b,c,*], Zhong Lin Wang[a,b,c,d,*], Zhou Li[a,b,c,*]

[a] CAS Center for Excellence in Nanoscience, Beijing Key Laboratory of Micro-nano Energy and Sensor, Beijing Institute of Nanoenergy and Nanosystems, Chinese Academy of Sciences, Beijing 100083, PR China
[b] School of Nanoscience and Technology, University of Chinese Academy of Sciences, Beijing 100049, PR China
[c] Center on Nanoenergy Research, School of Physical Science and Technology, Guangxi University, Nanning 530004, PR China
[d] School of Materials Science and Engineering, Georgia Institute of Technology, Atlanta, GA 30332-0245, United States
[e] Beijing Institute of Graphic Communication, Beijing 102600, PR China

ARTICLE INFO

Keywords:
Implantable nanogenerator
Tunable biodegradation
Au nanorods
Near-infrared
Photothermal

ABSTRACT

Implantable triboelectric nanogenerators (iTENGs) are promising to work as sustainable power source for implanted healthcare electronic devices. In this study, we fabricated a serial of biodegradable (BD) iTENGs and effectively tuned their degradation process *in vivo* by employing Au nanorods (AuNRs), which responded to the near-infrared (NIR) light sensitively. The implanted BD-iTENG worked well for more than 28 days *in vivo*, without NIR treatment. When NIR treatment was applied, the output of AuNRs-BD-iTENG rapidly reduced to 0 within 24 h and the device was mostly degraded in 14 days. This showed that the *in vivo* degradation of our BD-iTENG could be triggered and come into effect very quickly with rational manipulation. The peak value of *in vitro* and *in vivo* output voltage generated by the AuNRs-BD-iTENG were 28 V and 2 V, respectively. Moreover, the *in vivo* output voltage was applied on fibroblast cells and demonstrated a significant acceleration for cell migration across the scratch, which was very beneficial to wound healing process. In addition, we discovered that the alternating BD-iTENG output was as efficient as direct current (DC) stimuli. The mechanisms were investigated. Our work has demonstrated the feasibility of building a photothermally tunable BD-iTENG as a transient power source for biomedical healthcare electronics.

1. Introduction

Over the past decades, implantable electronic devices have made tremendous strides in health monitoring and medical treatment fields [1–4]. Batteries are traditional power sources for these devices, however, they have intrinsic drawbacks, such as limited life-span and heavy weight, which put forward a giant challenge for energy storage and supply [5]. Since the last decades, piezoelectric and triboelectric nanogenerators (PENGs and TENGs) working as power sources have attracted great attentions because they can effectively convert mechanical energy into electric power [6–15]. High-performance flexible PENGs have been demonstrated to collect energy from heart, lungs, chest or muscles of living mice, adult Yorkshire porcine or rats [16]. Zheng et al. demonstrated the applications of TENG for *in vivo* biomechanical energy harvesting in rats and swine [17]. Apart from electrical energy generation, PENG and TENG can also work in wearable devices [18–20]

For implantable healthcare devices which are aimed at short-term treatment, bio-degradability has been proposed as an important requirement, because it can avoid the surgery to remove the devices after the accomplishment of their work cycles [21–23]. In addition, a tunable degradation process is highly welcome. Till now, several types of biodegradable-TENGs (BD-TENGs) have been developed [24–27]. Zheng et al. reported a BD-TENG using combinations of degradable polymers which were degraded completely after 9 weeks implantation in rats and showed no negative effects [24]. Also, Yao et al. fabricated high-

* Corresponding authors at: CAS Center for Excellence in Nanoscience, Beijing Key Laboratory of Micro-nano Energy and Sensor, Beijing Institute of Nanoenergy and Nanosystems, Chinese Academy of Sciences, Beijing 100083, PR China.
E-mail addresses: lilinlin@binn.cas.cn (L. Li), zhong.wang@mse.gatech.edu (Z.L. Wang), zli@binn.cas.cn (Z. Li).
[1] These authors contributed equally to this work.

https://doi.org/10.1016/j.nanoen.2018.10.020
Received 3 September 2018; Received in revised form 30 September 2018; Accepted 11 October 2018
Available online 23 October 2018
2211-2855/

performance and biodegradable TENGs using functioned cellulose nanofibrils [25]. Wang et al. fabricated chitosan-based TENGs; and the chitosan films were engineered with various materials and treated by laser to enhance their outputs [27]. These reported BD-TENGs are promising to be applied in animal bodies without adverse effects. However, only few of them have been actually investigated *in vivo*, and none of them have ever developed tunable degradation approaches.

One of the most powerful approaches to manipulate *in vivo* responses is near-infrared (NIR) treatment [28–30]. The NIR photothermal effect based on Au nanorods (AuNRs) has been extensively studied and applied in cancer inhibition and drug delivery fields [31–33]. However, AuNRs based NIR photothermal approaches have never been tested in TENGs yet. There are many challenges to execute it. First, the working principle of TENGs is based on triboelectrification and electrostatic induction, and the addition of AuNRs may interfere the friction and electrostatic process. Second, the addition of AuNRs may enhance the difficulty of encapsulation. Third, after encapsulation and implantation into bodies, whether the NIR treatment can still work properly is unknown.

In this study, we fabricated a tunable BD implantable TENG (BD-iTENG) responding to NIR photothermal manipulation, and investigated their biomechanical energy conversion and bio-degradation process both *in vivo* and *in vivo*. The comparison between several kinds of biodegradable devices with our BD-iTENG were listed on Table 1. By adopting a hemisphere-array (HA) based structure, not only the contact area of the two friction layers was enlarged, but also a spacer between them was omitted. This enabled a persistent and unattenuated output in long terms, which was a great advantage over the spacer-based TENG. In addition, the Au-doped PLGA film in BD-iTENG endowed our BD-iTENGs the ability to respond to NIR irradiation, so that the biodegradation process can be rationally controlled. These are the two most outstanding features of our BD-iTENG, especially compared to the previous reported iTENG in ref [24]. The *in vitro* open-circuit voltage (*Voc*) of the BD-iTENG reached 28 V, and the corresponding short-circuit current (*Isc*) reached 220 nA. After implantation, the *Voc* was about 2 V in rats. This BD-iTENG showed controllable biodegradable process by employing AuNRs to respond the NIR treatment. Without AuNRs doping and NIR, the BD-iTENG worked well for more than 28 days *in vivo*. With Au nanorods doping and NIR treatment, the output of the BD-iTENG rapidly reduced to 0 within 24 h, and the device was largely degraded in 14 days *in vivo*. The output of the iTENG was applied on the L929 cells and significantly accelerated the process of cells migration across the scratch, which was crucial for wound healing treatment. Our work demonstrated the feasibility of building BD-iTENG as a tunable, transient and implantable power source for medical treatments.

2. Experimental section

2.1. Fabrication of Au nanorods

Colloidal gold nanorods were synthesized according to a modified version of the seed-growth method developed by Jana and co-worker [34–36]. The seed solution consisted of 5 mL of 0.2 M cetyltrimethylammonium bromide (CTAB) solution mixed with 5 mL of 0.0005 M $HAuCl_4$. 0.6 mL of ice-cold 0.01 M $NaBH_4$ were added to the stirred solution. Vigorous stirring of the seed solution was continued for 2 min. After stirring, the solution was kept at 25 °C. The growth solution was prepared with 50 mL of 0.001 M $HAuCl_4$ and 50 mL of 0.001 M CTAB, and after gentle mixing of the solution, 30 μL of 0.0788 M ascorbic acid was added [37]. In the final step, 12 μL of the seed solution was added to the growth solution. The size of gold nanorods were determined by using transmission electron microscopy (TEM).

2.2. Fabrication of Au doped PLGA, PCL & PLA layer

PLGA (50:50, Sigma-Aldrich) was dissolved in chloroform at a concentration of 5% (w/v). 1 M AuNRs was added into PLGA solution and stirred vigorously and cast on a glass plate with a dimension of D = 9 cm. The solution was air-dried for 12 h and then placed in a heat oven for another 12 h to exclude the remaining solvent. PCL (mg = 45000, Sigma-Aldrich) and PLA (mg = 45,000–55,000, Sigma-Aldrich) films were fabricated using the same method as PLGA. The thickness of the as-fabricated layers was about 50–100 μm.

2.3. Preparation of Poly (1,8-octanediol-co-citric acid) (POC)

All chemicals were purchased from Sigma-Aldrich (Milwaukee, WI). Following the previous method for synthesis of POC, equimolar amounts of citric acid and 1, 8-octanediol were added to a 250 mL three-neck round-bottom flask fitted with an inlet and outlet adapter. The mixture was melted under a flow of nitrogen gas by stirring at 160–165 °C in a silicon oil bath, and then the temperature of system went down to 140 °C [38,39]. The mixture was stirred for another hour at 140 °C to make the pre-polymer solution. The solution was poured out into a polytetrafluoroethylene beaker as quickly as possible. The pre-polymer was added into a polydimethylsiloxane (PDMS) template and post-polymerized at 80 °C under vacuum (1 Pa) for 1 d to create POC with a certain degree of cross-linking.

2.4. Fabrication of the hemispheres-array-structured films

The replication process was schematically depicted in Fig. S1. First, oxygen plasma treatment was conducted on a SiO_2/Si substrate for enhancing hydrophilicity and cleaning the surface. Then, polystyrene

Table 1
Summary of the reported and our biodegradable TENGs.

Literature	Zheng et al. [24]	Yao et al. [25]	Liang et al. [26]	Wang et al. [27]	Our work
Friction materials	PLGA/PHBV/PCL/PVA	CNFs/FEP	PVA/SA	Chitosan based film/ Kapton	PLGA/PCL/PLA
Encapsulation materials	PLGA/PHBV/PCL/PVA	None	Soluble adhesive tape	None	PLGA
Separation structure	Spacer	Spacer	None	None	Hemisphere array
Output	40 V/1μA	30 V/90μA	1.47 V/3.9 nA	13.5 V/42 nA	28 V/220 nA
Workable in liquid	Yes	No	No	No	Yes
Cell experiment *in vitro*	Yes	No	No	No	Yes
Animal experiment *in vivo*	Yes	No	No	No	Yes
Biological effects	Nerve repair	None	None	None	Tissue repair
Biodegradability of the whole TENG device	Yes	None	Yes	None	Yes
Control of biodegradation time	Choice of different polymers	None	None	None	Choice of different polymers; NIR treatment

(PS) spheres with diameters of 500 mm (Polysciences, Inc.) was coated onto the SiO_2/Si substrate to fabricate the PS template consisting of a monolayer of PS spheres. PDMS (Sylgard 184, Dow Corning) solution was poured onto the periodically arranged PS spheres, and allowed to solidify in an oven at 80 °C for 2 h. Then the PDMS template was detached from the SiO_2/Si substrate, and soaked in toluene for 24 h in order to remove the PS spheres. After that, a Cu film was sputtered onto the top surface of the PDMS mold. Then, POC was poured on top to replicate the PDMS mold. Finally, the cured POC was peeled off the PDMS mold and the POC HA structure was obtained. An electrode layer was deposited by the sputtering of gold (100 W, 30 min) on the HA structure.

2.5. Fabrication of BD-iTENG

The BD-iTENG was composed of three parts. First, the Au-deposited hemispheres-array-structured layer served as both the triboelectric material and the bottom electrode. Second, the Biodegradable Polymer 1 (BDP1) layer was the other triboelectric layer and magnesium was deposited on the top side to serve as top electrode. Third, The BDP2 doped with AuNRs was applied as bottom substrate. The top and bottom parts were sealed with BDP solutions.

2.6. Encapsulation of BD-iTENG

PLGA encapsulation was done by immersing the as-fabricated BD-iTENG into high concentration (10%, w/v) PLGA solution and let it air-dried overnight. Furthermore, the device was sealed by a heat sealer to exclude any interstice. This procedure also applied to PLA & PCL encapsulation.

2.7. Electrical measurements: in vitro test

A liner motor was employed as the external force to drive the BD-iTENG (operating distance, 50 mm; maximum speed, 1 m s^{-1}; acceleration, 1 m s^{-2}; deceleration, 1 m s^{-2}). The V_{OC} was measured by an oscilloscope (HDO6104), the I_{SC} and the transferred charge were detected by an electrometer (Keithley 6517B).

2.8. Electrical measurements: in vivo test

To measure the electrical signal of BD-iTENGs *in vivo*, we implanted

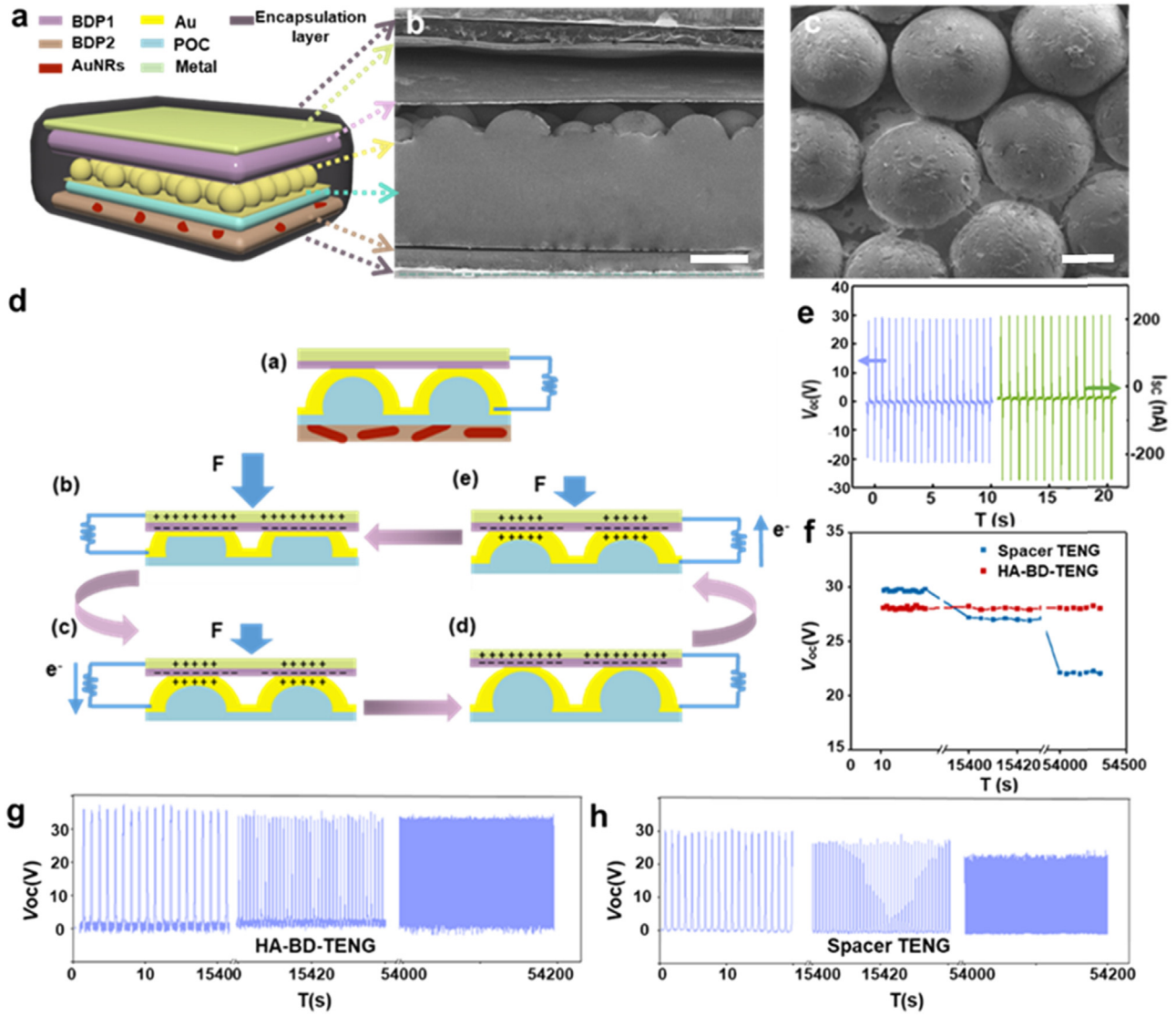

Fig. 1. (a) Structure design of the photothermal-controlled biodegradable triboelectric nanogenerator (BD-iTENG). (b) Section view of BD-iTENG (scale bar: 500 μm). (c) Top view SEM image of POC-HA (scale bar: 200 μm). (d) Working principle of the BD-iTENG. (e) Open-circuit voltage (V_{OC}) and Short-circuit current (I_{SC}) of BD-iTENG. (f) Stability of spacer-based iTENG and as fabricated HA-iTENG. (g-h) The output of the HA-iTENG (g) and spacer-iTENG (h) at 1 Hz for 54,200 s.

the BD-iTENG in the subdermal region on the back of the SD rats. This implant region can facilitate our subsequent measurements and avoid the wires being destroyed by rats scratching. Finger tapping was applied to the subdermal iTENG when measuring the outputs.

2.9. NIR treatment

For both *in vitro* and *in vivo* experiment, our BD-iTENGs were exposed to a near infrared laser of 808 nm for 1 h per day, with a power of 5.2 W cm^{-2}.

2.10. Cell culture

The L929 cells were cultured in DMEM high glucose medium containing 10% fetal bovine serum (FBS) and 1% penicillin/streptomycin at 37 °C under 5% CO_2. After incubation for 3 d, the L929 cells were passaged once.

2.11. Cell viability

The different BD layers were sterilized with 75% ethyl alcohol and placed in 96-well cell plate. The biocompatible of BD layers were determined using a standard methylthiazolyl tetrazolium (MTT, Sigma Aldrich) assay for cell viability measurement. Briefly, L929 cells were seeded in 96-well cell culture plate at 1×10^4 per well until adherent and then incubated for 1–3 d. All the other operations were the same as described above. Error bars were based on standard deviations of at least quadruplicate measurements.

2.12. Cell scratch experiment

The L929 cells were cultured in 6-well cell plate with interdigital electrode embeded for 24 h. Afterward, the samples were stained with 1, 1′-dioctadecyl-3, 3, 3′, 3′-tetramethylindocarbocyanine perchlorateand (DiI) for 20 min in dark. After removing the DiI dye, a scratch was made on the conflunt L929 cells using a piptte tip, then different EF were applied on the cells. The cells were examined using the Lecia confocal fluorescence microscope (LECIA TCS SP8).

3. Result and discussion

3.1. Fabrication of BD-iTENGs

We fabricated the BD-iTENG by adopting a HA based structure [40]. The as-fabricated BD-iTENG included friction layers, back electrodes, AuNRs layer and encapsulation layer (Fig. 1a,b). The HA friction layer consisted of POC, and a thin film of Au was deposited on top of the POC HA to serve as one electrode. POC-HA was prepared by a template-based method (Fig. S1). As shown in Fig. 1c and Fig. S2, the POC-HA with uniform structure and an average diameter of 500 μm was formed. The POC-HA not only enlarged the contact area of the two friction layers, but also omitted the necessity of using a spacer between them. Biodegradable Polymer 1 (BDP1) was the other friction layer and a thin film of Mg was deposited on its back as the other electrode. BDP2 was the specially designed AuNRs-containing layer in our BD-iTENG, which was placed under the POC-HA structure. The aim of BDP2 layer was to bring in AuNRs for the iTENG, and the BDP2 layer was made from the

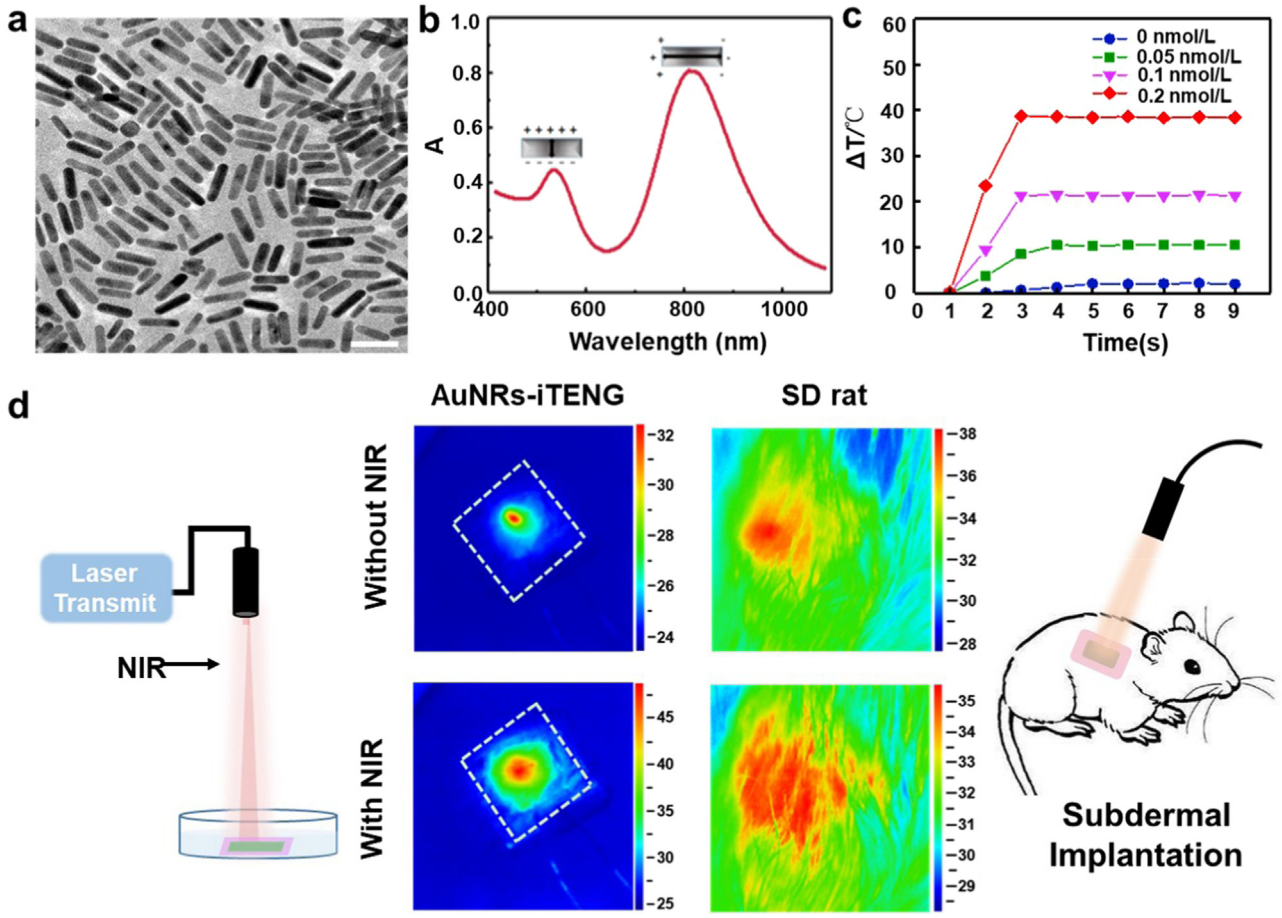

Fig. 2. (a) HR-TEM of Au nanorods (scale bar: 20 nm). (b) Absorbance of Au nanorods with wavelength from 400 nm to 1100 nm using UV–vis spectrometer spectra of Au nanorods. (c) Temperature variation of Au nanorods solution irradiated by NIR laser with a power density of 5.2 W cm^{-2}. (d) Infrared thermal imaging of AuNRs-BD-iTENG *in vitro* and after implantion in SD rats.

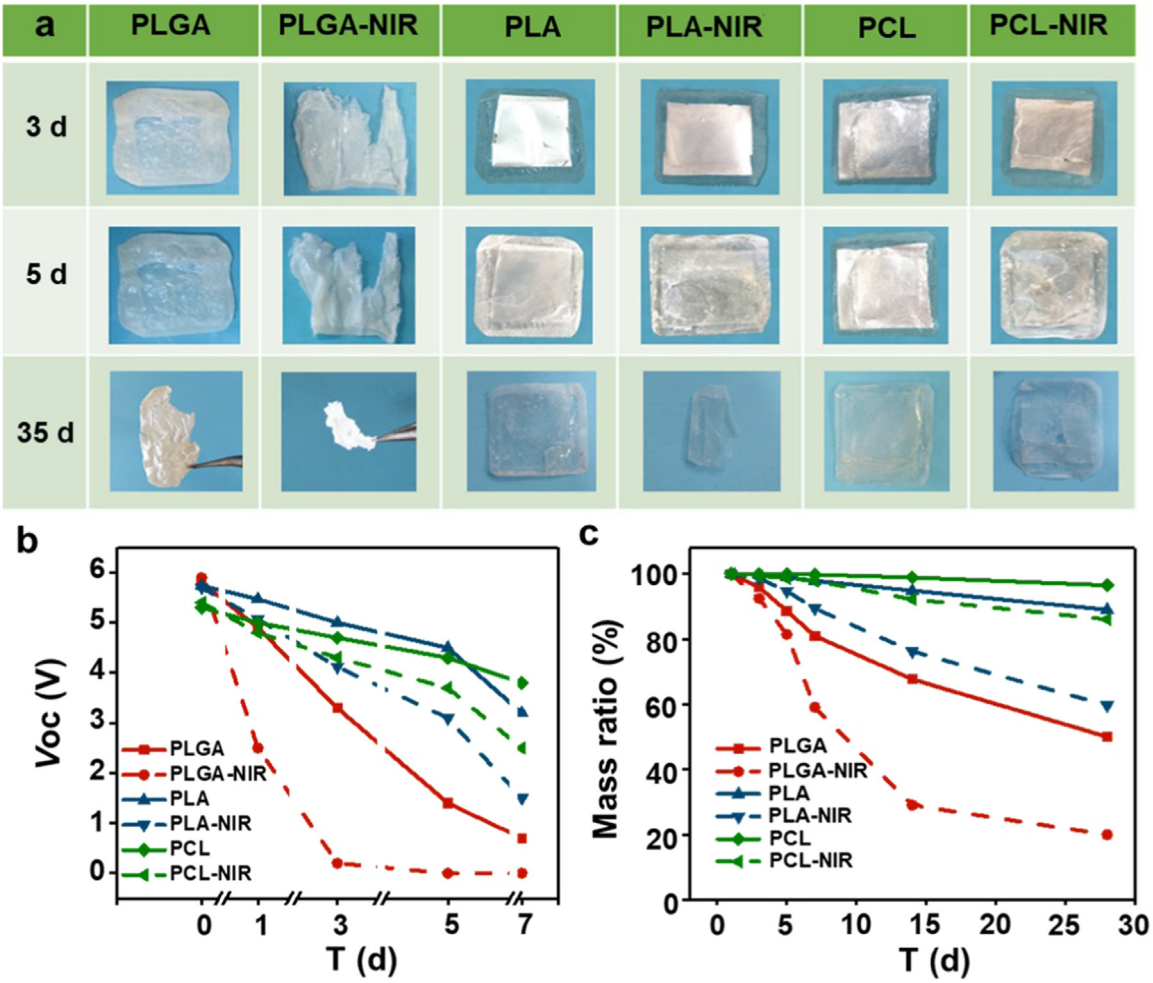

Fig. 3. *In vitro* degradation evaluation of various BD-iTENG (size, 1.2 cm × 1.2 cm; thickness, 0.65 mm) under different conditions. BDP2 layers of those iTENG were all doped with AuNRs. (a) Biodegradation of the BD-iTENG made from PLGA, PLA and PCL in PBS at 37 °C with or without NIR laser. (b) Voltage output of the three kinds of BD- iTENGs with or without NIR treatment in 35 d. (c) Mass variation of the three kinds of BD- iTENGs with or without NIR treatment in 35 d.

same material as BDP1. Then the device was encapsulated using the same material of BDP1 and BDP2. The BD materials tested in this study included: poly (L-lactide-*co*-glycolide) (PLGA), poly (caprolactone) (PCL) and polylactic acid (PLA), which all had good biocompatibility and flexibility [21].

The working mechanism of the as-fabricated BD-iTENG was schematically presented in Fig. 1d. The electricity-generating process had been described as the vertical contact separation mode of TENG [41,42]. When a compressive force was applied to the BD-iTENG, the Au-POC-HA deformed and fully contacted with BDP1. Oppositely charged surfaces were created due to the different electron affinity of Au-POC-HA and BDP1 layer. Once the compressive force disappeared, the Au-POC-HA tended to return to its original structure and became less contacted with BDP1 layer. A potential drop between the Au layer and Mg back electrode impelled the free electrons transferred from one electrode to another to balance the electrostatic field. When the contact decreased from maximum to minimum, the potential drop stemmed from the triboelectric charges disappeared gradually. When the compressive force was applied to Au-POC-HA and BDP1 again, the induced electrons flowed back and created a reverse current. The periodically compression and release of Au-POC-HA and BDP1 layer resulted in an AC output signal in the external circuit.

To test the *in vitro* electric performance of the BD-iTENG in air, a mechanical linear motor was applied on the BD-iTENG at 1 Hz. The open circuit voltage (V_{OC}) and short circuit current (I_{SC}) reached 28 V and 220 nA, respectively (Fig. 1e). The quantity of the electrical charge was 12 nC (Fig. S3). We also fabricated a TENG composed of the same materials and layers, but the POC layer and BDP1 layer were separated by a foam spacer. After 54200 measurements, the BD-iTENG retained 98.7% of the initial voltage output (Fig. 1g), while the spacer-based iTENG declined to 73.3% of its original voltage (Fig. 1h). This demonstrated that the HA-based BD-iTENG had a better stability than the spacer-based ones (Fig. 1f). Therefore, the as-fabricated BD-iTENGs were suitable to serve as long-term electric devices.

3.2. Photothermal property of the AuNRs

The core modulation of the degradation process relies on the doping of AuNRs in BDP2 layer. The conversion efficiency of NIR to heat energy increased with the decreasing size of AuNRs [43]. The AuNRs in this study were fabricated using seed-growth solution method (Fig. S4). Theyy were highly uniform and homogeneous, and had a good dispersibility in seed-growth solution. The AuNRs had an average length of 22 nm and an aspect ratio of 3.3 (Fig. 2a and Fig. S5). The longitudinal and lateral plasmon resonances of AuNRs were around 805 nm and 520 nm respectively (Fig. 2b). Fig. 2c showed the temperature rise in the AuNRs solutions after treated by NIR laser (808 nm, 5.2 W cm^{-2}), and the photothermal effect was stronger when the concentration of the AuNRs solution was higher. The time required to reach the plateau decreased from 5 s to 2.8 s as the concentration increased from 0 to 0.2 nmol L^{-1}. The temperature change (ΔT) increased from 3 °C to 40 °C when the concentration increased from 0 to 0.2 nmol L^{-1}. Considering

the actual temperature tolerance of Sprague Dawley (SD) rat, the concentration of 0.1 nmol L^{-1} was selected as the optimal concentration for doping the BDP2 layer in the following experiment. The photothermal effect of the BD-iTENG was also measured (Fig. 2d). After tuned by the NIR laser for 5 min, the temperature of the *in vitro* BD-iTENG increased by 13.2 °C. For the AuNRs-BD-iTENG after implantation and NIR modulation, the highest temperature was not changed very much, but the heated region increased significantly. The NIR laser (808 nm, 5.2 W cm^{-2}) caused no damage to the skin and surrounding tissue (Fig. 2d).

3.3. *In vitro* controllable degradation of BD-iTENGs

We fabricated a serial of BD-iTENGs using three kinds of materials: PLGA, PCL and PLA. For each kind of iTENG, BDP1, BDP2 and the encapsulation layer were all made using the same materials and the BDP2 all layers were doped with AuNRs. As shown in Fig. S6, the fabricated BD-iTENG has a size of 1.2 × 1.2 cm^2, a thickness of 0.65 mm and a weight of 0.075 g. The iTENG was immersed in Phosphate Buffered Saline (PBS) at 37 °C *in vitro* for 35 d. As shown in Fig. 3a, without NIR treatment, the PLGA, PLA and PCL iTENG devices all kept their integrated structure at the early stage (0–3 d). After 5 d, PLGA-iTENG showed a noticeable deformation in structure. The other two devices still maintained their integrated structure. After 35 d, most parts of PLGA-iTENG were degraded due to the hydrolysis of PBS. Although the other two devices retained their overall shape, they showed obvious deformation and material loss. With NIR treatment, the degradation rate of all these BD-iTENG devices were obviously accelerated, especially for the PLGA-iTENG. The integrated structure of PLGA-iTENG was destroyed at an early stage (3 d). After 35 d, the

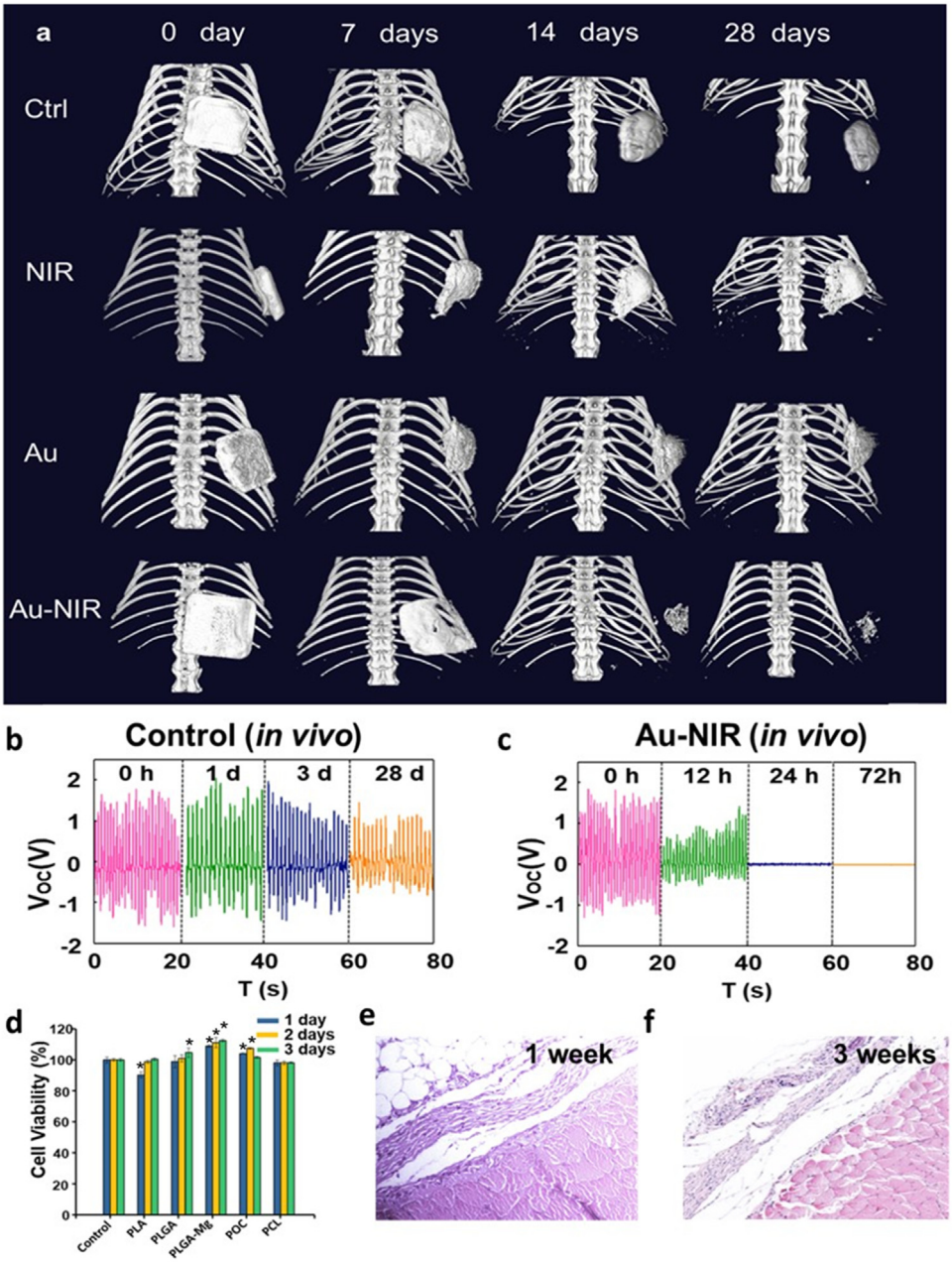

Fig. 4. Degradation *in vivo*. (a) Micro-CT image of the implanted PLGA-iTENGs at various time points. (b) The electrical output of the PLGA-iTENG without AuNRs or NIR. (c) The electrical output of the PLGA-iTENG with AuNRs and NIR. (d) Cell viability after cells were cultured with different BDP layers for 3 d. (Note: * $p < 0.05$) (e-f) Histological section of tissue at the implant sites, excised after 1 and 3 weeks, respectively.

integrated structures of all the encapsulated iTENGs were visibly destroyed, and parts of these iTENGs disappeared. The V_{OC} of the iTENGs with and without NIR were recorded in Fig. 3b. Without NIR treatment, the V_{OC} of the PLGA-iTENG decreased slowly from 6 V to 0.3 V in 7 d. In comparison, with NIR treatment, the V_{OC} decreased obviously faster from 6 V to 0.2 V in 3 d. The detailed outputs of PLGA-iTENG with or without NIR treatment were shown in Fig. S7. For PLA and PCL-iTENG, the output V_{OC} reduced to about 4.8 V in 5 d without NIR treatment; when applying NIR treatment, the output reduction was more in PLA than in PCL. The changes of mass of these iTENG devices were shown in Fig. 3c. The retained mass of PLGA-iTENG was reduced from 100% to 17.3% after 35 d of NIR. Without NIR treatment, the retained mass was 38.2% after 35 d. The retained output and masses of these iTENG devices all followed this trend: PLGA > PLA > PCL either with or without NIR treatment, while NIR treatment evidently accelerated the degradation process. With these results, we demonstrated that one way to modulate the degradation time was the choice of BD materials. ITENGs made from PLGA were very prone to degrade while those made from PCL were much more resistant in a solution environment. More specifically, the adoption of AuNRs and NIR light permitted us to control the degradation process more actively. After applying NIR light, the working of PLGA-iTENG was stopped within 3 days *in vitro*.

3.4. *In vivo* tunable degradation of BD-iTENG

To demonstrate that the BD-iTENG can work properly and efficiently *in vivo*, we evaluated the PLGA-iTENGs degradation after implanting them into the subdermal region of SD rats. The devices were sterilized by irradiation (^{60}Co/25 kGy) before implantation, and the procedure strictly followed the "Beijing Administration Rule of Laboratory Animals" and the national standards of "Laboratory Animal Requirements of Environment and Housing Facilities (GB 14925–2001)."

After implantation, computed tomography (CT) imaging was carried

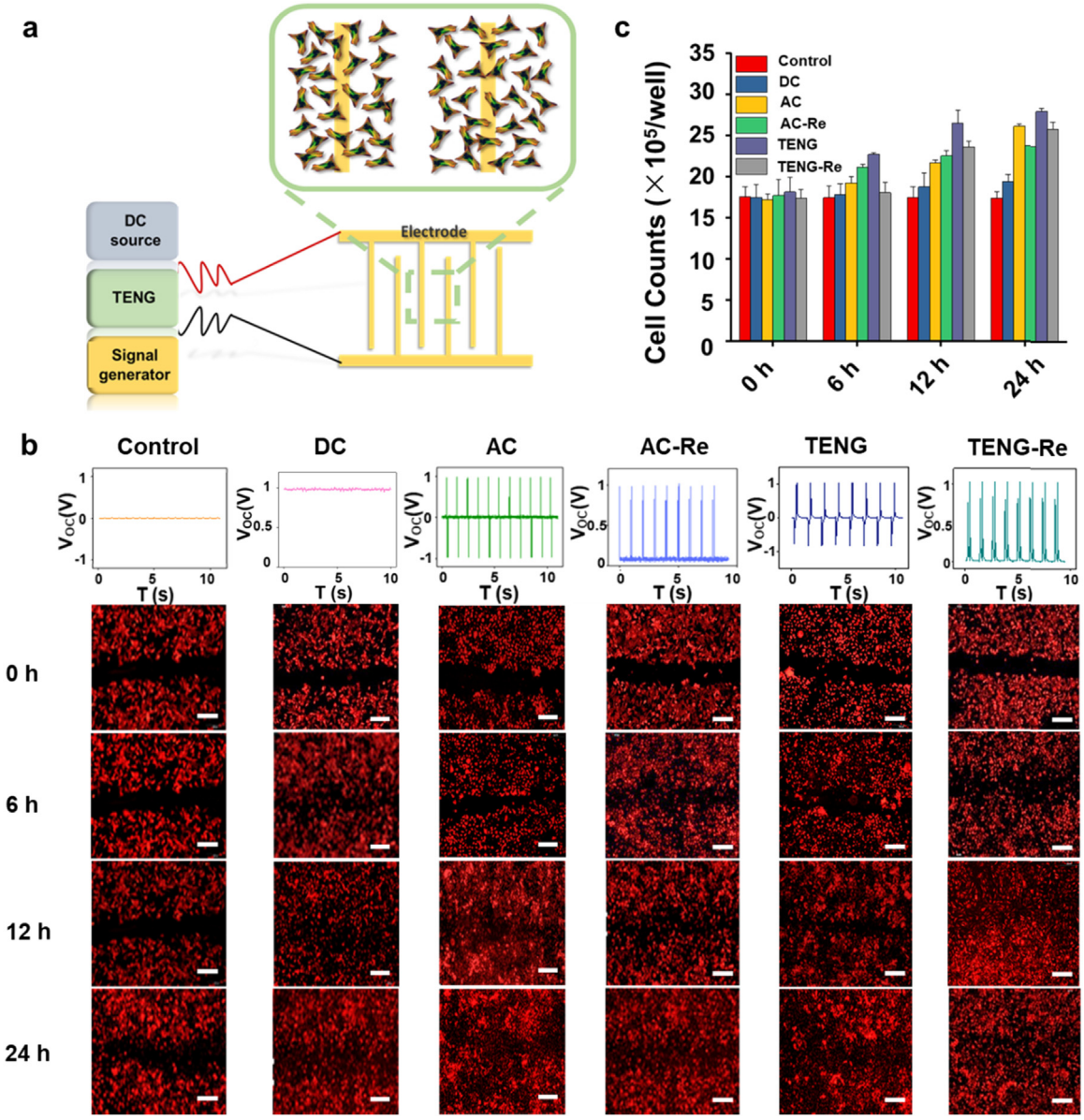

Fig. 5. Electrical stimulation of fibroblast L929 cells by DC, AC, and BD-iTENG. (a) Schematic diagram of the electrical stimuli setup using PDMS encapsulated interdigital electrodes for our BD-iTENG and other power sources. (b) Fluorescence microscope images of cells migration after electrical field (EF) stimulation. The EF promoted the L929 cells to migrate and fill the scratch. Scale bars: 100 μm. The DC and AC were applied at voltage of 1 V or ± 1 V. (c) Cell proliferation in the 24 h was enhanced in EF groups as tested by a cell counter.

out to monitor the degradation of PLGA-iTENG *in vivo* for 28 days (Fig. 4a). CT images showed that for the control PLGA-iTENG with neither AuNRs nor NIR treatment, the devices remained intact in 28 days. The PLGA-iTENG without AuNRs doping but with NIR treatment retained their shape on the 7th day, but some holes appeared on the edge of the device on the 14th day, and the holes became enlarged on the 28th day. For the PLGA-iTENG with AuNRs doping but no NIR treatment, some burr appeared on the edge of the device from the 14th day onward. For the PLGA-iTENG with both AuNRs and NIR treatment, large holes appeared on the 7th day, and the device gradually degraded into small fragments in 14 days.

Their output performances were also recorded (Figs. 4b, 4c and S8). The *in vivo* TENG voltage output was generated by applying finger tapping on the rat skin underneath which our BD-iTENG had been implanted at 1 Hz (as shown in Video 1). The PLGA-iTENG without AuNRs doping and NIR worked very steadily for more than 3 day ($Voc > 90\%$ and $Isc > 95\%$). Meanwhile it persisted about 70% of the *Voc* and 50% of the *Isc* on the 28th day after implantation (Fig. 4b and S9a). As for the PLGA-iTENG which contained AuNRs and treated by NIR laser, the voltage markedly decreased from 1.8 to 0.5 V at the 12th hour after only one NIR treatment; and the output decreased to 0 after 24 h *in vivo* (Fig. 4c). Furthermore, the current only maintained 30% of its original state after 12 h and almost disappeared in 72th hour. The output of PLGA-iTENG with only AuNRs or NIR was shown in Fig. S8. Because the working principle of TENG depends on the coupling between triboelectric effect and electrostatic induction, the output can be easily disturbed by liquids. Once the degradation of PLGA encapsulation layer results in any penetrating crack, water will permeate into the device. The water will disturb the electrostatic induction between the friction layers and erode the Mg electrode. In this circumstance the output of the TENG will decrease greatly with no visible damage observed in the structure of the TENG. Therefore the performance drop is nonlinearly dependent on the structural degradation.

Supplementary material related to this article can be found online at doi:10.1016/j.nanoen.2018.10.020.

After 3 weeks of iTENG implantation, the surgery wound healed well, and no obvious infection was detected, revealing good biocompatibility of the PLGA-iTENG (Fig. 4). In fact, all the BD materials used in this study were highly biocompatible [21]. To verify the biocompatibility of the BD materials, they were cut into small pieces, placed in 96-well plates, and L929 cells were seeded in the BD materials containing wells at 1×10^4 cells per well. Then they were incubated for 3 d and the cell viability was examined each day (Fig. 4d). Each group showed very good viability (over 90.3%) in the 3 days of culture as compared to the control group at the same day, and some of them (PLA, PLGA, PLGA-Mg) even enhanced the cell proliferation (over 100%). After sacrificing the rats, tissue slides were obtained and examined. The histological section staining results showed that the BD-iTENG was located between the subdermal layer and the muscle layer, and surrounded by a small amount of fibrous tissue, and no significant inflammatory reaction was detected (Fig. 4e and Fig. 4f). These results suggested that the BD-iTENGs were highly bio-compatible and suited to serve as implantable devices.

3.5. Tissue Repairing using BD-iTENG

Electrical stimulations have become efficient approaches for many clinical disease treatments, including heart failure, spine injury and wound healing [44–48]. However, each treatment requires specific electrical parameters to promote recovery. It's very crucial that the outputs of the electrical devices are suited for the requirements of different treatments. Here we investigated the feasibility of our BD-iTENG to be applied as an energy source to enhance wound healing.

Fig. 5a showed the electrical stimulation setup in this experiment. The electrical field (EF) was delivered from power sources (DC power system, alternating current (AC) power system, or iTENG) to the cells by interdigital electrodes. The interdigital electrodes were fabricated by Cu deposition; the width of each electrode was 10 μm and the interval in between was 100 μm. The interdigital electrodes were encapsulated by a layer of PDMS, the depth of which was about 200 μm. The L929 cells were cultured on top of the PDMS. As shown in Fig. 5a, a scratch was made in the confluent L929 cells using a 20 μL pipette tip.

Immediately, the electrical stimulation was applied to the cells in each group except for the control group. In this study, we used different electric signals including DC, AC, alternating current rectified (AC-Re), iTENG and iTENG-Re to stimulate the L929 cells. According to previous studies, DC EF within the range of 100–200 mV mm^{-1} were verified to promote the cell migrations. In those studies, the electrical stimuli were delivered to the cells using electrostatic chambers, which were based on electrical currents [49,50]. The current in the system was about 1 mA. However, the iTENG current output was usually 500 nA to 5 μA. Therefore, in our work, we designed the PDMS-encapsulated interdigital electrodes to provide iTENG stimuli to the cells. PDMS was an insulative material, therefore, only the electrical potential of the iTENG was delivered to the cells. This design could cut off the shortage of the low current of iTENG. To achieve the effective EF of 100 mV mm^{-1}, only 1 V output was required, which was very easy for our BD-iTENG to make. The calculation of EF was done using COMSOL as shown in Fig. S11.

After the scratch was made for 6 h, all electrical groups showed obvious cell migration towards the middle of the scratch, while the scratch remained the same in the control group. After 24 h treatment, all the electric groups cells had converged at the middle of the scratch, making the scratch almost invisible; while in the control group only a few cells migrated to the margins of the scratch (Fig. 5b).

We used another four different electric signals: AC, AC-Re, iTENG and iTENG-Re, besides previously studied DC supplier. We found that the alternating output groups, AC and iTENG showed equal or even better enhancement in cells migration for wound healing, which had rarely been reported before. To investigate the migration enhancing mechanism of AC and iTENG outputs, cell proliferation results were carried out as shown in Fig. 5c. In this part, a culture medium containing 5% FBS was used to prohibit cell proliferation. The cell counts without electrical stimulation didn't increase within 24 h, demonstrating that cell proliferation didn't happen. On the contrary, the cells proliferation was enhanced more or less in all the electrically stimulated groups, with DC group being the least and iTENG group being the most. This result suggested that for DC group, the enhancement of scratch healing was mostly due to the direct migration of cells induced by the constant EF. More interestingly, for AC and iTENG groups, the contributions of their EF may come from two aspects. One was from the EF induced migration tendency. Although the EF was in an alternating mode, the alternating EF didn't counteract with each other, but promoted the cell migration from the two margins of the scratch one after the other in sequence. The second contribution was the enhanced cell proliferation, which made the scratch to recover more efficiently. According to the results, all the EF imposed on the interdigital electrodes played an effective role in cell migration enhancement, and BD-iTENG without rectification performed the best. Therefore, our BD-iTENG is highly promising to be applied in wound healing treatment.

4. Conclusion

In summary, we have fabricated a serial of BD-iTENGs and successfully demonstrated a controlled degradation process *in vivo*. The *in vitro Voc* and *Isc* of the BD-iTENG were 28 V and 220 nA, respectively. After implantation, the *in vivo Voc* was 2 V in rats. Our BD-iTENG gained tunable biodegradable process by employing AuNRs to respond the NIR. Without AuNRs doping and NIR treatment, the BD-iTENG worked well for more than 28 days *in vivo*. When applying NIR treatment to the implanted AuNRs- BD-iTENG, the output rapidly reduced to 0 within 24 h, and the device was mostly degraded in 14 days *in vivo*.

The output of the iTENG was applied on the fibroblast cells, and significantly accelerated the process of cells migration across the scratch, which was crucial for wound healing treatment. In addition, we discovered that alternating iTENG output was more efficient than traditional DC stimuli to enhance wound healing, and investigated the mechanisms. Our work demonstrated the feasibility of building BD-iTENG as a tunable transient power source for implantable healthcare electronics.

Acknowledgments

The authors thank the support of National Key R&D project from Minister of Science and Technology, China (2016YFA0202703), National Natural Science Foundation of China (No. 61875015, 31571006, 81601629 and 21801019), Beijing Talents Fund (2015000021223ZK21), the Beijing Natural Science Foundation (2182091) and the National Youth Talent Support Program.

Appendix A. Supporting information

Supplementary data associated with this article can be found in the online version at doi:10.1016/j.nanoen.2018.10.020.

References

[1] R. Hinchet, S.-W. Kim, Wearable and implantable mechanical energy harvesters for self-powered biomedical systems, ACS Nano 9 (2015) 7742–7745.
[2] G. Hwang, V. Annapureddy, J.H. Han, D.-J. Joe, C. Baek, D.Y. Park, D.H. Kim, J.H. Park, C.K. Jeong, K. Park, J. Choi, D.K. Kim, J. Ryu, K.J. Lee, Self-powered wireless sensor node enabled by an aerosol-deposited PZT flexible energy harvester, Adv. Energy Mater. 6 (2016) 1600237.
[3] F.A. Hassani, W. Peh, G. Gammad, R.P. Mogan, T.K. Ng, T. Kuo, L.G. Ng, P. Luu, S.-C. Yen, C. Lee, A three-dimensionally (3D) printed implantable device for voiding the bladder using shape memory alloy (SMA) actuators, Adv. Sci. 4 (2017) 1700143.
[4] X. Xie, Z. Wen, Q. Shen, C. Chen, M. Peng, Y. Yang, N. Sun, P. Cheng, H. Shao, Y. Zhang, Q. Zhu, X. Chen, X. Sun, Impedance atching effect between a triboelectric nanogenerator and a piezoresistive pressure sensor induced Self-powered weighing, Adv. Mater. Technol. 3 (2018) 1800054.
[5] A. Azhim, J. Yamaguchi, Y. Hirao, Y. Kinouchi, H. Yamaguchi, K. Yoshizaki, S. Ito, M. Nomura, Monitoring carotid blood flow and ECG for cardiovascular disease in elder subjects, Conf. Proc. IEEE Eng. Med. Biol. Soc. 5 (2005) 5495–5498.
[6] U. Khan, T.-H. Kim, H. Ryu, W. Seung, S.-W. Kim, Graphene tribotronics for electronic skin and touch screen applications, Adv. Mater. 29 (2017) 1603544.
[7] J.H. Park, G.-T. Hwang, S. Kim, J. Seo, H.-J. Park, K. Yu, T.-S. Kim, K.J. Lee, Flash-induced self-limited plasmonic welding of silver nanowire network for transparent flexible energy harvester, Adv. Mater. 29 (2017) 1603473.
[8] H. Zhang, X.-S. Zhang, X. Cheng, Y. Liu, M. Han, X. Xue, S. Wang, F. Yang, S.A. Shankaregowda, H. Zhang, Z. Xu, A flexible and implantable piezoelectric generator harvesting energy from the pulsation of ascending aorta: in vitro and in vivo studies, Nano Energy 12 (2015) 296–304.
[9] X. Pu, H. Guo, J. Chen, X. Wang, Y. Xi, C. Hu, Z.L. Wang, Eye motion triggered self-powered mechnosensational communication system using triboelectric nanogenerator, Sci. Adv. 3 (2017) e1700694.
[10] G.J. Zhang, Q.L. Liao, Z. Zhang, Q.J. Liang, Y.L. Zhao, X. Zheng, Y. Zhang, Novel piezoelectric paper-based flexible nanogenerators composed of batio3 nanoparticles and bacterial cellulose, Adv. Sci. 3 (2016) 1500257.
[11] H. Guo, M.-H. Yeh, Y.-C. Lai, Y. Zi, C. Wu, Z. Wen, C. Hu, Z.L. Wang, All-in-one shape-adaptive self-charging power package for wearable electronics, ACS Nano 10 (2016) 10580–10588.
[12] H. Feng, C. Zhao, P. Tan, R. Liu, X. Chen, Z. Li, Nanogenerator for biomedical applications, Adv. Healthc. Mater. 7 (2018) e1701298.
[13] Q. Shen, X. Xie, M. Peng, N. Sun, H. Shao, H. Zheng, Z. Wen, X. Sun, Self-powered vehicle emission testing system based on coupling of triboelectric and chemoresistive effects, Adv. Funct. Mater. 28 (2018) 1703420.
[14] H. Ouyang, J. Tian, G. Sun, Y. Zou, Z. Liu, H. Li, L. Zhao, B. Shi, Y. Fan, Y. Fan, Z.L. Wang, Z. Li, Self-powered pulse sensor for antidiastole of cardiovascular disease, Adv. Mater. 29 (2017) 1703456.
[15] H. Li, X. Wang, W. Jiang, H. Fu, X. Liang, K. Zhang, Z. Li, C. Zhao, H. Feng, J. Nie, R. Liu, G. Zhou, Y. Fan, Z. Li, Alkali metal chlorides based hydrogel as eco-friendly neutral electrolyte for bendable solid-state capacitor, Adv. Mater. Interfaces 5 (2018) 1701648.
[16] X. Cheng, X. Xue, Y. Ma, M. Han, W. Zhang, Z. Xu, H. Zhang, H. Zhang, Implantable and self-powered blood pressure monitoring based on a piezoelectric thin film: simulated, in vitro and in vivo studies, Nano Energy 22 (2016) 453–460.
[17] Q. Zheng, H. Zhang, B. Shi, X. Xue, Z. Liu, Y. Jin, Y. Ma, Y. Zou, X. Wang, Z. An, W. Tang, W. Zhang, F. Yang, Y. Liu, X. Lang, Z. Xu, Z. Li, Z.L. Wang, In vivo self-powered wireless cardiac monitoring via implantable triboelectric nanogenerator, Acs Nano 10 (2016) 6510–6518.
[18] Z. Wen, Y. Yang, N. Sun, G. Li, Y. Liu, C. Chen, J. Shi, L. Xie, H. Jiang, D. Bao, Q. Zhuo, X. Sun, A wrinkled PEDOT: PSS film based stretchable and transparent triboelectric nanogenerator for wearable energy harvesters and active motion sensors, Adv. Funct. Mater. 28 (2018) 1803684.
[19] Y. Yang, N. Sun, Z. Wen, P. Cheng, H. Zheng, H. Shao, Y. Xia, C. Chen, H. Lan, X. Xie, C. Zhou, J. Zhong, X. Sun, S.-T. Lee, Liquid-metal-based super-stretchable and structure-designable triboelectric nanogenerator for wearable electronics, ACS Nano 12 (2018) 2027–2034.
[20] C. Zhou, Y. Yang, N. Sun, Z. Wen, P. Cheng, X. Xie, H. Shao, Q. Shen, X. Chen, Y. Liu, Z.L. Wang, X. Sun, Flexible self-charging power units for portable electronics based on folded carbon paper, Nano Res. 8 (2018) 4313–4322.
[21] S.W. Hwang, C.H. Lee, H. Cheng, J.W. Jeong, S.K. Kang, J.H. Kim, J. Shin, J. Yang, Z. Liu, G.A. Ameer, Y. Huang, J.A. Rogers, Biodegradable elastomers and silicon nanomembranes/nanoribbons for stretchable, transient electronics, and biosensors, Nano Lett. 15 (2015) 2801–2808.
[22] D.H. Kim, J. Viventi, J.J. Amsden, J. Xiao, L. Vigeland, Y.S. Kim, J.A. Blanco, B. Panilaitis, E.S. Frechette, D. Contreras, D.L. Kaplan, F.G. Omenetto, Y. Huang, K.C. Hwang, M.R. Zakin, B. Litt, J.A. Rogers, Dissolvable films of silk fibroin for ultrathin conformal bio-integrated electronics, Nat. Mater. 9 (2010) 511–517.
[23] C.H. Wang, C.Y. Hsieh, J.C. Hwang, Flexible organic thin-film transistors with silk fibroin as the gate dielectric, Adv. Mater. 23 (2011) 1630–1634.
[24] Q. Zheng, Y. Zou, Y. Zhang, Z. Liu, B. Shi, X. Wang, Y. Jin, H. Ouyang, Z. Li, Z.L. Wang, Biodegradable triboelectric nanogenerator as a life-time designed implantable power source, Sci. Adv. 2 (2016) e1501478.
[25] C. Yao, A. Hernandez, Y. Yu, Z. Cai, X. Wang, Triboelectric nanogenerators and power-boards from cellulose nanofibrils and recycled materials, Nano Energy 30 (2016) 103–108.
[26] Q.J. Liang, Q. Zhang, X.Q. Yan, X.Q. Liao, L.H. Han, F. Yi, M.Y. Ma, Y. Zhang, Recyclable and Green Triboelectric Nanogenerator, Adv. Mater. 29 (2016) 1604941.
[27] R. Wang, S. Gao, Z. Yang, Y. Li, W. Chen, B. Wu, W. Wu, Engineered and laser-processed chitosan biopolymers for sustainable and biodegradable triboelectric power generation, Adv. Mater. 30 (2018) 1706267.
[28] X. Sun, C. Wang, M. Gao, A. Hu, Z. Liu, Remotely controlled red blood cell carriers for cancer targeting and near-infrared light-triggered drug release in combined photothermal-chemotherapy, Adv. Funct. Mater. 25 (2015) 2386–2394.
[29] Q. Yuan, Y. Wu, J. Wang, D. Lu, Z. Zhao, T. Liu, X. Zhang, W. Tan, Targeted bioimaging and photodynamic therapy nanoplatform using an aptamer-guided G-quadruplex DNA carrier and near-infrared light, Angew. Chem. Int. Ed. 52 (2013) 13965–13969.
[30] M.P. Melancon, M. Zhou, C. Li, Cancer theranostics with near-infrared light-activatable multimodal nanoparticles, Acc. Chem. Res. 44 (2011) 947–956.
[31] M.R. Ali, S.R. Panikkanvalappil, M.A. El-Sayed, Enhancing the efficiency of gold nanoparticles treatment of cancer by increasing their rate of endocytosis and cell accumulation using rifampicin, J. Am. Chem. Soc. 136 (2014) 4464–4467.
[32] E.T. Castellana, R.C. Gamez, M.E. Gomez, D.H. Russell, Longitudinal surface plasmon resonance based gold nanorod biosensors for mass spectrometry, Langmuir 26 (2010) 6066–6070.
[33] N. Li, Z. Yu, W. Pan, Y. Han, T. Zhang, B. Tang, A. Near-Infrared Light-Triggered, Nanocarrier with reversible DNA valves for intracellular controlled release, Adv. Funct. Mater. 23 (2013) 2255–2262.
[34] X.C. Ye, C. Zheng, J. Chen, Y.Z. Gao, C.B. Murray, Using binary surfactant mixtures to simultaneously improve the dimensional tunability and monodispersity in the seeded growth of gold nanorods, Nano Lett. 13 (2013) 765–771.
[35] M. Liu, P. Guyotsionnest, Synthesis and optical characterization of Au/Ag core/shell nanorods, J. Phys. Chem. B 108 (2004) 5882–5888.
[36] K. Mitamura, T. Imae, N. Saito, O. Takai, Fabrication and self-assembly of hydrophobic gold nanorods, J. Phys. Chem. B 111 (2007) 8891–8898.
[37] S.-C. Hsiao, J.-L. Ou, Y. Sung, C.-P. Chang, M.-D. Ger, Preparation of sulfate- and carboxyl-functionalized magnetite/polystyrene spheres for further deposition of gold nanoparticles, Colloid and Polym. Sci 288 (2010) 787–794.
[38] C.G. Jeong, S.J. Hollister, Mechanical, permeability, and degradation properties of 3D designed poly(1,8 octanediol-co-citrate) scaffolds for soft tissue engineering, J. Biomed. Mater. Res. B Appl. Biomater. 93 (2010) 141–149.
[39] J. Yang, A.R. Webb, G.A. Ameer, Novel citric acid-based biodegradable elastomers for tissue engineering, Adv. Mater. 16 (2010) 511–516.
[40] K.Y. Lee, H.-J. Yoon, T. Jiang, X. Wen, W. Seung, S.-W. Kim, Z.L. Wang, Fully packaged self-powered triboelectric pressure sensor using hemispheres-array, Adv. Energy Mater. 6 (2016) 1502566.
[41] G. Zhu, Z.H. Lin, Q. Jing, P. Bai, C. Pan, Y. Yang, Y. Zhou, Z.L. Wang, Toward large-scale energy harvesting by a nanoparticle-enhanced triboelectric nanogenerator, Nano Lett. 13 (2013) 847–853.
[42] Z.L. Wang, Triboelectric nanogenerators as new energy technology for self-powered systems and as active mechanical and chemical sensors, ACS Nano 7 (2013) 9533–9557.
[43] X. Huang, S. Neretina, M.A. El-Sayed, Gold nanorods: from synthesis and properties to biological and biomedical applications, Adv. Mater. 21 (2009) 4880–4910.
[44] D.C. Wescott, M.N. Pinkerton, B.J. Gaffey, K.T. Beggs, T.J. Milne, M.C. Meikle, Osteogenic gene expression by human periodontal ligament cells under cyclic tension, J. Dent. Res. 86 (2007) 1212–1216.
[45] T. Kanno, T. Takahashi, W. Ariyoshi, T. Tsujisawa, M. Haga, T. Nishihara, Tensile mechanical strain up-regulates Runx2 and osteogenic factor expression in human periosteal cells: implications for distraction osteogenesis, J. Oral. Maxillofac. Surg. 63 (2005) 499–504.
[46] L. Tang, Z. Lin, Y.M. Li, Effects of different magnitudes of mechanical strain on

Osteoblasts in vitro, Biochem. Biophys. Res. Commun. 344 (2006) 122–128.
[47] J. Zhang, J.H. Wang, Mechanobiological response of tendon stem cells: implications of tendon homeostasis and pathogenesis of tendinopathy, J. Orthop. Res. 28 (2010) 639–643.
[48] W. Guo, X. Zhang, X. Yu, S. Wang, J. Qiu, W. Tang, L. Li, H. Liu, Z.L. Wang, Self-powered electrical stimulation for enhancing neural differentiation of mesenchymal stem cells on graphene- poly(3,4-ethylenedioxythiophene) hybrid microfibers, ACS Nano 10 (2016) 5086–5095.
[49] M. Griffin, S.A. Iqbal, A. Sebastian, J. Colthurst, A. Bayat, Degenerate wave and capacitive coupling increase human MSC invasion and proliferation while reducing cytotoxicity in an in vitro wound healing model, Plos One 6 (2011) e23404.
[50] M. Zhao, B. Song, J. Pu, T. Wada, B. Reid, G. Tai, F. Wang, A. Guo, P. Walczysko, Y. Gu, T. Sasaki, A. Suzuki, J.V. Forrester, H.R. Bourne, P.N. Devreotes, C.D. McCaig, J.M. Penninger, Electrical signals control wound healing through phosphatidylinositol-3-OH kinase-gamma and PTEN, Nature 442 (2006) 457–460.